Journal of Alloys and Compounds 616 (2014) 5–13

Contents lists available at ScienceDirect

Journal of Alloys and Compounds

journal homepage: www.elsevier.com/locate/jalcom

The solidification behaviour of the UO_2–ThO_2 system in a laser heating study

R. Böhler [a,b], A. Quaini [c,1], L. Capriotti [c,a], P. Çakır [d,a], O. Beneš [a], K. Boboridis [a], A. Guiot [a], L. Luzzi [c], R.J.M. Konings [a], D. Manara [a,*]

[a] European Commission, Joint Research Centre, Institute for Transuranium Elements (ITU), P.O. Box 2340, 76125 Karlsruhe, Germany
[b] Delft University of Technology, Faculty of Applied Sciences, Department of Radiation Science and Technology, Mekelweg 15, 2629 JB Delft, Netherlands
[c] Politecnico di Milano, Department of Energy, Enrico Fermi Center for Nuclear Studies (CeSNEF), via La Masa 34, 20156 Milano, Italy
[d] Ege Univerity, Institute of Nuclear Sciences, 35100 Bornova Izmir, Turkey

ARTICLE INFO

Article history:
Received 7 April 2014
Received in revised form 4 July 2014
Accepted 7 July 2014
Available online 18 July 2014

Keywords:
Actinide alloys and compounds
Ceramics
Phase transitions
Phase diagrams
Thorium–uranium dioxide
Raman spectroscopy

ABSTRACT

The high-temperature phase diagram of the UO_2–ThO_2 system has been experimentally revisited in the present study for the first time since 1970, using a laser heating approach combined with fast pyrometry in a thermal arrest method. The melting/solidification temperature, which is of fundamental information for a reactor design was studied here. It was found that low addition of ThO_2 to UO_2 would result in a slight decrease of the solidification temperature. A minimum was found at 3098 K around a composition of 5 mol% ThO_2. The solid/liquid transition temperature was then observed to increase again with increasing ThO_2 fraction. The literature value of pure ThO_2 (around 3630 K) was well reproduced here. Important experimental difficulties, stemming from the high temperatures reached during the measurements, as well as a complete investigation with electron microscopy, Raman spectroscopy and powder X-ray diffraction, are extensively discussed. These results show the importance of the high-temperature oxygen chemistry in this actinide oxide compound.

1. Introduction

There is a renaissance of interest in thorium based fuels as an alternative to uranium based fuels in nuclear reactors. Thorium has advantages in terms of proliferation, waste management, supply and safety [1]. However, there are still technical and safety related issues to bring it to a fully commercial use [2–4]. UO_2–ThO_2 mixed fuels (or $(U,Th)O_2$; abbreviated here as TOX) have advantages with respect to proliferation resistance for nuclear weapons and long term waste concerns over pure UO_2 fuel [5–7]. One reason why the thorium containing fuels are possibly advantageous compared to pure UO_2 are their material properties, more specifically, the properties of ThO_2. ThO_2 is a highly stable oxide, not subjected to oxidation beyond the stoichiometric composition, and its thermal conductivity is higher than that of uranium dioxide [8]. These properties together with the very high melting temperature of ThO_2, constitute obvious advantages in terms of the in-pile fuel performance of TOX fuel [9] and also a rather stable and less radiotoxic form for the waste with less minor actinides [10]. But compared to UO_2 the $(U,Th)O_2$ mixed fuels are investigated rather poorly. Especially the high temperature properties are only investigated in earlier research by Lambertson et al. and Latta et al. [11,12]. Interestingly Latta et al. found a minimum temperature around 5 mol% ThO_2, but did not provide an explanation of this surprising deviation of ideal behaviour. The end-members of this system were studied more recently by Manara et al. (UO_2 [13]) and Ronchi and Hiernaut (ThO_2 [14]).

One of the main goals of the present work is to remeasure the full UO_2–ThO_2 pseudo-binary section, whereby the melting/solidification behaviour of these mixed oxides are studied by laser heating and fast pyrometry under controlled atmosphere. This setup has been used for measuring some high temperature phase changes of refractory materials (e.g. [13,15,16] revealing new results on the melting behaviour. First studies in mixed actinide oxide compounds, namely on mixed uranium-plutonium dioxides revealed also large differences to earlier believed ideal behaviour of this system at high temperatures [17]. New studies on the mixed $(U,Pu)O_2$ system confirmed these observations of a minimum temperature in the melting/solidification transition [18]. A conclusion obtained of the latter work is that the high temperature phase

* Corresponding author.
E-mail address: dario.manara@ec.europa.eu (D. Manara).
URL: https://ec.europa.eu/jrc/en/institutes/itu (D. Manara).
[1] Current address: CEA Saclay – CEA DEN / DANS / DPC / SCCME / LM2T, 91191 Gif-sur-Yvette Cedex, France.

http://dx.doi.org/10.1016/j.jallcom.2014.07.055
0925-8388/

transitions are sensitive to the oxygen potential and can be fully understood only in the light of ternary systems of the mixed oxide components [19,20]. ThO_2 in contrast is chemically more stable and has a lower oxygen potential than the other actinide oxides [21]. This makes it therefore chemically more stable also at high temperatures. Under those conditions it was interesting to check on one hand the high temperature behaviour of a nuclear fuel material, as well as, on the other hand, fundamental aspects of a system for which an essentially ideal solution behaviour can be foreseen at high temperatures.

The results of the laser melting experiments are completed with different methods as scanning electron microscopy (SEM), Energy-dispersive X-ray spectroscopy (EDX), X-ray diffraction (XRD) and Raman spectroscopy. Among these, Raman analysis of actinide compounds is a rather original method to investigate the material surfaces [22,23]. The UO_2–ThO_2 pseudo-binary phase diagram was finally refined with new experimental high temperature phase change data.

2. Description of the experiments

2.1. Sample preparation

The UO_2–ThO_2 mixed samples were prepared using a sol–gel external gelation method with different molar fractions of ThO_2 ($x(ThO_2)$ = 0.05, 0.20, 0.40, 0.60, 0.80, 0.95, 1.00). The different samples were identified with the label TOX and the amount-of-substance fraction $x(ThO_2)\cdot 100$. Chemically, the samples contained besides uranium and thorium negligible amounts of different metals (< 0.1 wt.%). The powder/sol–gel beads were produced by precipitation of the U/Th solution in small droplets. These beads were heated in air to remove the organics at 400°C. Then the sol–gel beads were calcined in quartz crucibles at 800 °C in air to remove the organics from the sol–gel process and convert the U–Th-hydroxide precipitation to form the $(U,Th)O_{2+x}$. After 2 h the gas is changed to Ar/H_2 to reduce the uranium back to U^{IV}. Finally, the powder is pressed to pellets of about 5 mm in diameter and 2–3 mm thickness. These pellets are sintered at 1650 °C for 8 h in $Ar/H_2$to obtain a O/M ratio of 2.00.

2.2. Laser melting experimental setup

The experimental apparatus used in this work is summarised in Fig. 1 and was already described in detail elsewhere [13]. The sample was mounted in a pressurized cell with a controlled atmosphere, which was inside an α shielding glovebox. The contact between the sample and its mount was minimized by radially arranged screws to hold the sample in place. With this approach the molten volume is contained by the outer periphery of colder solid material, thus, preventing contamination by foreign material, hence can be described as quasi – containerless. The power source for heating was a Nd:YAG continuous-wave laser radiating at 1064.5 nm. The laser is programmable with a power/time profile of variable duration as short as a few milliseconds and a maximum power of 4.5 kW. However the heating profile was kept simple in order to separate better power changes from a thermal signal response.

The samples were preheated with low laser powers (45 W or 90 W) for 30 s to reduce thermal shocks. After this time a sufficient steady state heat distribution through the sample with a measured front surface temperature of 1500–2000 K has established and the sample was brought to melting with pulses of different length (100 ms to 1 s) at a constant power plateau (up to 600 W). The chosen power depends also on the composition of the sample since ThO_2 is in the near infra-red (laser wavelength) nearly transparent. This transparency is temperature dependant and disappears at high temperature where absorption / emissivity values similar to other actinide dioxides are reached [14].

After each pulse the power was set back to the preheating value to let the sample re-solidify and reach again a homogeneous state before the next pulse was started. A maximum of 3 pulses were applied in a set of shots before letting the sample cool naturally. Such heating cycles were performed under air for compositions rich in ThO_2 and Ar for intermediate and UO_2-rich compositions. The buffer gas was slightly pressurized up to 0.3 MPa to reduce the vaporisation. The onset of melting was detected by the appearance of vibrations in the signal of a probe laser (Ar^+ cw 750 mW to 1.5 W) reflected by the sample surface (reflected-light-signal technique, or RLS) [24]. These vibrations disappear during the solidification process at the thermal arrest and therefore establish the temperature at the thermal arrest as the solidification temperature.

The surface radiance temperature in the centre of the heated zone was measured by a pyrometer operating at 652 nm and with a fast logarithmic amplifier. The nominal spot size was approximately 0.5 mm in diameter. The pyrometer was calibrated against a standard tungsten-ribbon lamp in the range 1800–2500 K, ensuring traceability to the International Temperature Scale of 1990 [25]. The validity of the calibration, the quality of the optical windows, the alignment, and the thermodynamic equilibrium conditions on the measurement spot were tested by measuring in-situ the well established melting radiance temperatures of UO_2 (3040 K [13]) and tungsten (3207 K [26]) close to 650 nm.

The true temperature was obtained by correcting the radiance temperature with the measured of the normal spectral emittance NSE ($\varepsilon(\lambda,T)$). A further spectrometer, based on a linear array of 256 photodiodes, was used to record the sample thermal radiance in the range of 488–1011 nm, whereby the time resolution is one spectrum per millisecond at best. The photodiode at 649 nm was calibrated up to 2500 K using the tungsten-ribbon lamp and this calibration was transferred to a tubular-cavity variable-temperature graphite blackbody furnace up to 3500 K. The remaining photodiodes were then calibrated with this blackbody, allowing a conversion of output signal to spectral radiance over the entire useful wavelength range.

The measured radiance spectra can be fitted with two physically equivalent methods: by a least-squares regression to Planck's distribution law or by the radiance temperature, T_λ, plotted as a function of wavelength, λ, assuming a grey body with constant wavelength independent emissivity $\varepsilon(T)$. Both methods were successfully applied on other actinide dioxides and are shown in detail elsewhere [16,27]. For UO_2 the already published data is used [28], while the high temperature value (0.870 ± 0.044) obtained during the present work with both fits was adopted for pure ThO_2. This is in agreement with earlier results of ThO_2 [14,29] and is also supported by analogy to emittance data of other similar dioxides [16,27]. The emittance study could not be performed on all compositions. A linear interpolation between the two NSE of UO_2 and ThO_2 was calculated, giving to the generic intermediate composition a weighted value related to the amount of the two pure components, which are shown in Table 1. This assumption seems reasonable especially considering the close emittance values of the two end members and agreed well with the calculated values for some intermediate compositions.

The sample surface was considered to be smooth, as supported by the good repeatability of the measured radiance temperatures upon freezing. The freezing temperature of TOX was determined from the cooling stage of the recorded thermograms, locating the corresponding thermal arrest. As often observed in rapid laser-heating experiments of such materials, and confirmed by numerical simulation [16], the heating stage often occurs too quickly to reveal an observable melting arrest during this phase of the thermal cycle but could be estimated with the help of the RLS.

Uncertainties of the measurements were calculated according to the error-propagation law, taking into account the uncertainty associated to pyrometer calibration, the emissivity, transmittance of the optical system and the accuracy in detecting the onset of vibrations in the reflected light signal. The estimated

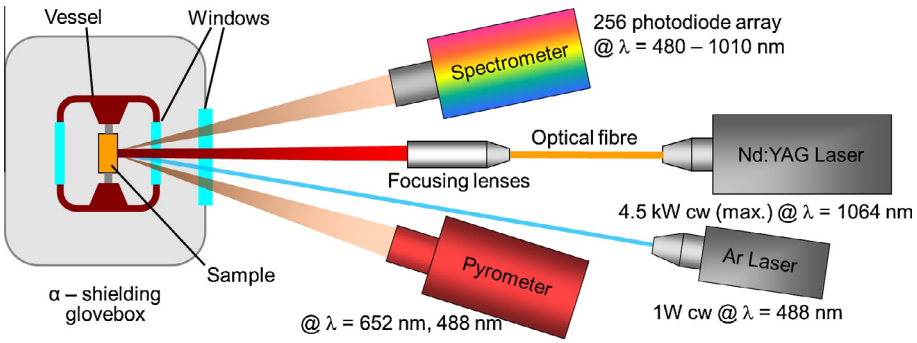

Fig. 1. A schematic description of the used apparatus for the melting experiments.

cumulative uncertainty is thus lower than ±2.5% of the reported temperatures in the worst cases for solidification temperatures and ±3.5% for melting transitions (calculated with a coverage factor $k = 2$).

2.3. Material characterisation

To check the composition, the material was investigated with different methods before and after the experiments. First, secondary electron (SE) and backscattered electron (BSE) images were recorded on a scanning electron micro-scope (SEM with a Philips XL40®) operated at 25 kV.

Additionally, the samples were characterized with a Bruker D8 advance® diffractometer (Cu Kα radiation), using a range of 10–120° with 0.009 steps. The procedure was later also conducted on re-solidified material to see a possible effect from melting.

The third method used to see possible effects on the surface was Raman spectroscopy. Raman spectra were measured with a Jobin–Yvon® T64000 spectrometer used in the single spectrograph configuration. The excitation source was a Coherent®cw laser (Ar^+ or Kr^+) radiating at wavelengths of 488 nm, 514.5 nm, 647 nm, and 752 nm with a nominal power up to several 100 mW at the exit of the cavity. The power impinging on the sample surface is lower by a factor 10 approximately and is chosen at each measurement in order to optimise the signal/noise ratio (by minimising the material fluorescence) and reducing undesirable oxidation/burning effects on the sample surface. Spectra are measured in a confocal microscope with a 50x magnification and long focal distance (about 1 cm). This feature gives a good signal / noise ratio independently of the surface shape, with a spatial resolution of 2×2 μm on the sample surface. The spectrograph angle is calibrated with the T_{2g} excitation of a silicon single crystal, set at 520.5 cm^{-1}.

3. Results of the melting experiments

3.1. Mixed uranium-thorium dioxide

Fig. 2 is an example of the recorded thermograms during the heating and cooling cycles. A TOX 40 specimen is, as described before, heated up to a temperature of about 1500 K in an Ar atmosphere and then brought to melting with pulses of different duration. After the laser pulse the sample cools by radiation conduction to the environment. This cooling process is interrupted by the release of latent heat during solidification of the molten pool and results in a short stabilisation of temperature. After 3 high power pulses the sample is let cool to room temperature and another set of 3 shots with longer duration are used to melt the sample front side. In Fig. 2 thermograms of the pulses with the same length are overlapped. Differences in the heating rate are mostly attributed to crack formation in the sample disk and therefore changes in the thermal conduction in the sample. The melting process heals some cracks so that the cooling curves are repeatable over successive shots with different lengths. This implies that the samples are stable for numerous heating cycles and segregation effects, due to non-congruent vaporisation and melting, do not influence the solidification temperature in successive shots.

From these thermograms the solidification temperature is deduced at the cooling stage at the peak of the thermal arrest. An ideal flat arrest was not observed at constant temperature, since the molten surface solidifies very quickly and builds a crust upon the molten material in only a few milliseconds [18]. Therefore the thermograms can be interpreted as follows: after turning off the high power pulse, the molten surface reaches a slight undercooling until a crust of re-solidified material starts to cover the melt. During this solidification the latent heat, released during the crust formation, serves as a power source and raises the temperature on the surface. The temperature reaches a local maximum, while the surface solidifies entirely and a trapped molten pool is left inside the solid material. The re-solidification of the enclosed melt is continuous and releases heat to the surrounding material, up to the sample surface. Therefore the cooling process at the surface is slowed down until the melt in the inside has solidified at the last inflection.

The reflected blue-light-laser (RLS) helps to identify this solidification, as well as the melting process. In Fig. 2 the 1st derivative of the RLS of the first shot (black) is shown in blue. One sees clear changes in the signal at the end of the laser pulse (end of heating) and right afterwards at the same time as the local temperature maximum at the thermal arrest. Also on the heating side one can identify a weaker change, also described in earlier work [13,16,24,27], at the same time as the sample surface reaches the melting temperature.

Fig. 3 and Table 1 summarise the melting/solidification points observed with the different (U, Th)O_2 compositions investigated in this work. Within the experimental uncertainty the temperature remain the same for the melting and solidification, which confirms that segregation effects during the experiments, as described before, seem to have a minor influence. One can also observe that the (U, Th)O_2 pseudo binary system seems to have a minimum melting/solidification point around 5 mol% ThO_2.

3.2. Thorium dioxide

Melting experiments with pure ThO_2 were performed with the current approach in air, showing a melting temperature of 3624 K ± 86 K. This is in agreement, within the reported uncertainties, with the established value in literature (3651 K ± 17 K) [14]. Tests in different atmospheres (air and argon) showed colour changes as described by Ronchi and Hiernaut [14]. While the melted material surface stayed white in experiments in air, in argon the sample tended to become black after several shots. Preliminary thermogravimetry tests showed a hypostoichiometric change of the black material, confirming the existence of a link between oxygen losses and change in colour of the specimen of a more metallic sample as seen also before on calcium oxide [30]. However, the temperature measured in the tests with Ar-atmosphere did not show a statistically significant difference, as one can expect from calculated thermograms [21].

4. Discussion

4.1. Microscopy

The samples were analysed by secondary-electron-microscopy at different magnifications. A typical microscope image (Fig. 4)

Table 1
Normal spectral emittance (NSE), melting temperature detected by RLS and solidification points observed by thermal arrest analysis in this work on mixed (U, Th)O_2.

Composition	NSE	No. of shots	Melting temperature / K	Solidification temperature / K
UO_2	0.830	–	–	3126 K ± 55 K [18]
TOX 5	0.832	9	3100 K ± 62 K	3098 K ± 54 K
TOX 20	0.838	11	3175 K ± 105 K	3157 K ± 69 K
TOX 40	0.846	21	3371 K ± 68 K	3341 K ± 53 K
TOX 60	0.854	9	3467 K ± 125 K	3447 K ± 59 K
TOX 80	0.862	4	n.d.	3529 K ± 91 K
TOX 95	0.868	4	n.d.	3584 K ± 67 K
ThO_2	0.870	11	3624 K ± 108 K	3624 K ± 86 K

Note: n.d. – not detected.

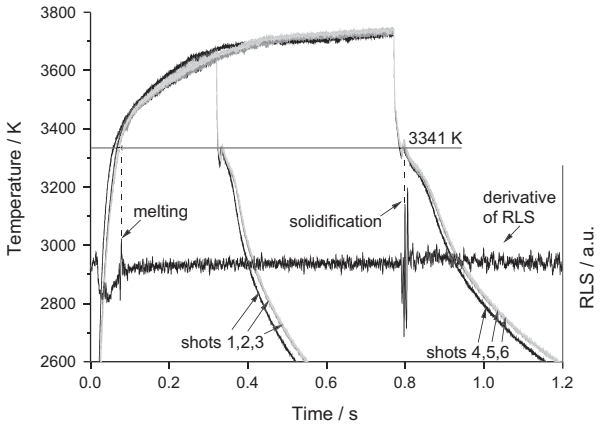

Fig. 2. Thermograms recorded on a single TOX 40 $(U_{0.60}Th_{0.40})O_2$ sample over 2 successive laser heating cycles. In each cycle the sample surface was hit by three high-power laser pulses (starting at 0 s) separated by dwelling periods of several seconds during which it was kept at an intermediate temperature around 1500 K in order to minimise thermal shocks. The solidification temperature of TOX 40 at 3341 K is suggested by the horizontal line. The reflected-light-signal (RLS) of shot 4 is shown below the corresponding thermogram indicating melting at about 0.08 s and 3370 K and solidification at 3341 K and 0.8 s.

shows the surface of a TOX 60 sample after the laser shots. One can see the edges of the melted and re-solidified zone of different successive shots. The EDX analysis showed no change of composition along the surface from the centre to the outside within the uncertainties of EDX. There is also no difference compared to the not melted material surrounding the re-solidified zone. In all analysed compositions there are no evident traces of segregation. The ratios U/Th in the re-solidified areas remain very close to the not melted one.

Since the EDX analysis has relatively large uncertainties (±10% in composition), further investigations were performed with Raman spectroscopy and powder X-ray diffraction analysis to confirm the absence of segregation effects.

4.2. Raman spectroscopy

Main purpose of the current Raman spectroscopy analysis was the detection of possible segregation/oxidation effects in the mixed oxide samples following the laser heating cycles beyond melting.

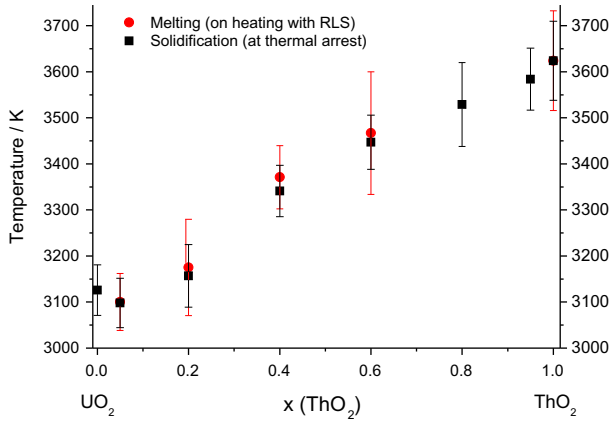

Fig. 3. The melting/solidification temperatures observed in the present work with help of RLS and thermal arrest analyses on different TOX samples. Vertical uncertainty bands combine the intrinsic instrumental uncertainty (pyrometer calibration, sample emissivity, transmittance of the optical system) with the experimental data spread.

Some Raman spectra recorded in this work with a 514 nm laser excitation source on mixed uranium–thorium dioxides are presented in Fig. 5.

The fluorite-like structures studied in this research (fcc, $Fm\bar{3}m$) have only one (triply degenerate) Raman active vibration (T_{2g}), which is taken as a reference peak for our investigation. In stoichiometric urania the peak is found at 445 cm^{-1} [31], in thoria at 465 cm^{-1} relative to the excitation wavelength [31]. This vibration is identified as zone "A" in the spectra reported in Fig. 5a. Zone "B" contains a rather weak peak around 575 cm^{-1}, which has been attributed to a longitudinal optical (LO) phonon [32]. Its Raman activity is linked to the presence of oxygen vacancies in the fcc fluorite lattice [33]. This peak is visible rather poorly in all compositions. Zone "C" contains, essentially in TOX 5 and TOX 20, a weak peak around 630 cm^{-1}. This feature has been assigned to the formation of oxygen interstitial clusters, resulting in the separation of a M_4O_9 super-symmetry within the fcc lattice [34]. The rather irregular features observable in zone "D" of the Raman spectra of Pure UO_2, TOX 5 and TOX 20, correspond to vibrations of species containing uranyl groups. These species (U_3O_7, U_3O_8, UO_3 [35]) can be easily formed on the sample surface in contact with air, especially under the irradiation of the laser used as excitation source for the Raman measurements. Obviously, the addition of ThO_2 (a chemically very stable compound) to UO_2 has a stabilising effect, with respect to the formation of these structures on the sample surface in contact with the air, only for compositions $x(ThO_2) > 0.2$ approximately. Finally, the presence of a broad and intense peak around 1150 cm^{-1} is clearly observable in zone "E" of the spectra measured in samples with $x(ThO_2) < 0.80$. This peak has been demonstrated to be an overtone of the 575 cm^{-1} LO phonon [32,36]. Its intensity obviously changes with composition. This peak was shown to be Raman resonant in uranium dioxide [32,36], but not in thorium dioxide. This explains its composition dependent behaviour in the current mixed oxides.

A plot of the dependence of the T_{2g} peak position with the ThO_2 content is shown in Fig. 6 and in Table 2. The average of several measurements on not melted and re-solidified material at the surface is shown with a combined uncertainty with a 2-k coverage factor resulting in a total uncertainty of 2–3 cm^{-1}(with a spectral uncertainty of ±1 cm^{-1}). The T_{2g} Raman shift clearly tends from urania to the thoria value following the amount of thoria in the material. This peak tends also to sharpen at increasing ThO_2 content, probably due to a decrease in oxygen defect concentration. The measurements were conducted on different spots at the surface showing no consistent (in-/decrease) and systematic (centre to outside) difference to each other on the same surface.

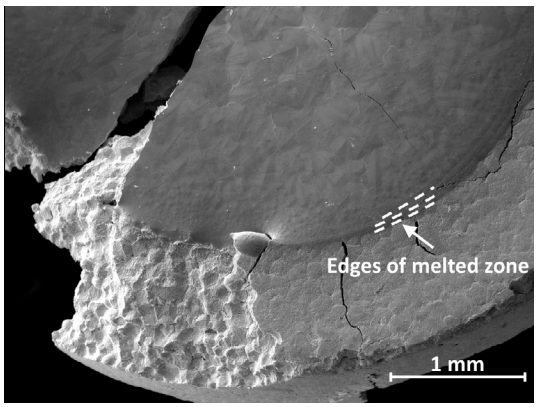

Fig. 4. Secondary electron image of a broken TOX 60 sample, with defined re-solidified zones from different successive shots.

This homogeneity of the surface could originate from the very fast formation of the crust combined with slow diffusion in the solid.

No full analytical relation between the composition and the T_{2g} peak Raman shift has been determined for this system. The T_{2g} peak wavenumber increases with an approximately linear trend only from pure UO_2 to 80 mol% ThO_2 for the not melted material. For higher thoria contents, this Raman mode keeps very similar to the one of pure ThO_2, both in peak position and intensity. This behaviour is probably attributable to the resonant nature of the T_{2g} Raman active mode in thorium dioxide, and its much higher scattering efficiency compared to UO_2 [37,38]. One can see that the re-solidified material has a consistently higher T_{2g} peak position than the not melted material, though very little around the end-members (UO_2 and ThO_2). An increase in the Raman shift would indicate a composition shift towards ThO_2 on the surface of the re-solidified material, compared to the not melted material for the intermediate compositions (with 20, 40 and 60 mol% ThO_2).

There are different effects which might play a role in the current observations with Raman spectroscopy: (i) high temperature lattice disorder, as Frenkel pairs in the oxygen sublattice [39], quenched to room temperature, could have an increasing effect on the peak shifts of the re-solidified material, (ii) changes of the material fractions as a result of different surface tensions in the melt or (iii) segregation can occur during the rapid heating/cooling cycles across the non-congruent melting transition, resulting in compositional shifts in the quenched solid, also (iv), the T_{2g} Raman scattering efficiency of ThO_2 is higher compared to UO_2 [37,38].

In order to detect possible effects of high-temperature surface oxidation or oxygen defect formation Fig. 5b shows the comparison between a broader Raman spectrum recorded with a 514 nm excitation laser on a re-solidified and a not melted TOX 60 sample. The most appreciable difference between the two spectra is the slight shift in the T_{2g} peak (see inset), corresponding to the difference in its position reported in Fig. 6. As mentioned above, such difference can be related to both a local enrichment in ThO_2, probably due to segregation during the melting/freezing process, and the formation/annihilation of oxygen defects. However, the slight differences in the spectral zones C and D of Fig. 5a, between 600 and 950 cm^{-1}, seem more reasonably attributable to variations in the background noise than to any clear formation or annihilation of oxygen defects during the thermal cycles beyond melting. It can be concluded that no obvious oxidation effects on the re-solidified surface could be detected by the current Raman analysis. Instead, this analysis revealed the occurrence of some segregation leading to non-negligible ThO_2 enrichment, with respect to the initial sample composition, in re-solidified samples with intermediate values of x(ThO_2). The lower relative intensities of the Raman peaks at 575 cm^{-1} and 1150 cm^{-1} in the re-solidified sample (Fig. 6) confirm the same trend, when compared with the spectra displayed in Fig. 5a for the various UO_2-ThO_2 compositions. Such segregation, occurring during the fast heating/cooling cycles, can be limited to the very external part of the sample surface. This part has been shown to be the first to solidify from the liquid forming a thin crust in contact with the external atmosphere [18]. It is the most likely to display segregation phenomena, due to slow diffusion in the solid [13,18]. However, its exact thickness has not been determined.

The penetration depth for the current Raman analysis can be conservatively assumed with the Lamber-Beer law to be 0.5 μm to a few μm (depending on the ThO_2 content)[40,41], compared to melted depth of at least 20 μm [16]. Therefore the analysis is certainly limited to a superficial layer considerably thinner than the whole melted pool and to a thinner layer than an EDX analysis, which has an emission depth of about 5 μm. It is not obvious to conclude whether the Raman-analysed part is smaller or bigger than the superficial crust initially formed upon solidification. Independently, it is plausible to assume that segregation effects observed by Raman spectroscopy in melted samples with intermediate x(ThO_2) values can be limited to an external layer of the refrozen pool. There, a composition enriched in ThO_2 can be formed and quenched at the beginning of the fast solidification process, according to the UO_2–ThO_2 solidus–liquidus phase boundaries.

In order to investigate the occurrence of similar segregation and additional oxidation phenomena in the whole mass of not melted and re-solidified material, powder X-ray analysis was performed.

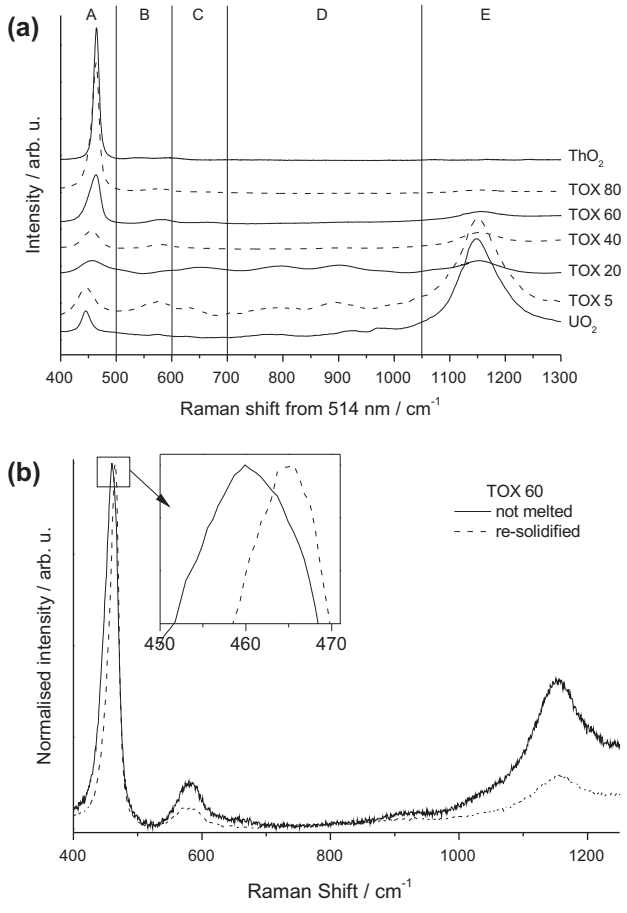

Fig. 5. Raman spectra recorded with a 514 nm excitation laser: (a) comparison of not melted samples with different ThO_2 content, and (b) comparison of a re-solidified and not melted TOX 60 sample.

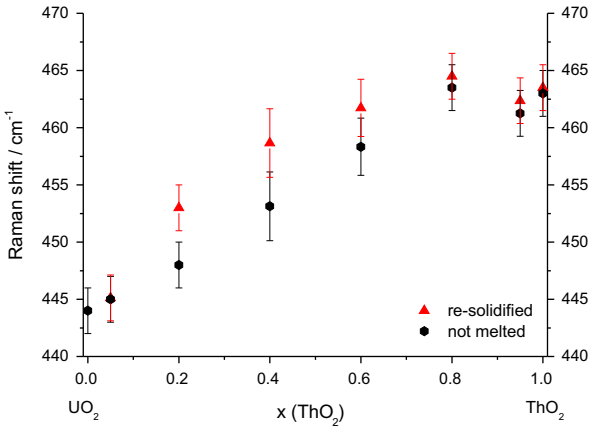

Fig. 6. Dependence of the Raman T_{2g} position on molar fraction of ThO_2.

Table 2
The evolution of T_{2g} positions and lattice parameter with ThO_2 content.

Composition	Raman shift/cm^{-1}		Lattice parameter/Å	
	Not melted	Re-solidified	Not melted	Re-solidified
UO_2	444	–	5.4708	–
TOX 5	445.1	445.1	5.4775	5.4780
TOX 20	448.1	453.0	5.4985	5.5031
TOX 40	452.9	458.6	5.5243	5.5245
TOX 60	458.3	461.7	5.5501	5.5513
TOX 80	463.5	464.5	5.5735	5.5747
TOX 95	461.3	462.4	5.5898	5.5900
ThO_2	463.0	463.5	5.5971	5.5972

4.3. Powder X-ray diffraction

Table 2 shows the measured lattice parameters obtained by powder X-ray diffraction (PXRD), while Fig. 7 shows the difference of the lattice parameter to the interpolation (Vegard's law) between the pure components ThO_2 and UO_2. One can easily see that the re-solidified and not melted material shows nearly identical lattice parameters. As well, no other (higher oxide) phases as the fcc $Fm\bar{3}m$ phase of the solid solution of (U, Th)O_2 – even on different samples in the uranium rich part – were seen in the diffraction patterns. The lattice parameter agree well with the parameters of Cohen and Berman [42] or Hubert et al. [44], except a slight deviation in Cohen and Berman's work from Vegard's law, showing a minimum at 2 mol% ThO_2. A small phase separation was seen for the re-solidified TOX 40, with a higher lattice parameter (5.5489 Å; +0.0288 Å away form Vegard's law), which is probably formed while cooling. Such segregation is explained in the next section in more detail with the help of the phase diagram.

The slight deviation to Vegard's law here can be attributed to uncertainty (of approximately 2%) in the initial composition or a slight change of the O/M ratio, although it is not possible to distinguish between these two effects only by the lattice parameter. Compared to the results from mixed (U, Pu)O_2 [43] or from hyperstoichiometric studies on (U, Th)O_2 [42], the change in O/M can be assumed to be small in this work. There is no study so far to the knowledge of the authors, which addresses the reduction of (U, Th)O_2. It is not surprising that due to the low oxygen potential of ThO_2 shifts in the lattice parameter caused by stoichiometric changes would be small. In some compositions an increase of the lattice parameters in the re-solidified material suggests a shift towards ThO_2, but is still within the uncertainty range and relatively small compared to the shifts indicated by Raman spectroscopy in this work. One has also to bear in mind that these measurements were done at room temperature and even though the samples are cooled down from high temperature very quickly and structures might be quenched, changes cannot be ruled out during cooling. Also, any local differences within the re-solidified zone are not seen by PXRD and are maybe averaged, especially since in the analysis no distinction of material close to the surface and "deeper" material can be made.

Finally, PXRD analysis confirms, with the before mentioned constraints, that the shift observed in the T_{2g} Raman peak of samples with intermediate x(ThO_2) values are probably attributable to UO_2–ThO_2 segregation limited to a very shallow region starting from the most external crust of the melted and re-solidified surface. The remaining re-solidified bulk maintains, within the experimental uncertainties, the initial composition even after the laser heating cycles beyond melting.

4.4. Melting temperature results

The melting point for ThO_2 is here measured to be 27 K lower than formerly measured and published by Ronchi and Hiernaut [14]. With the considered uncertainties, the difference is largely covered. In fact, by reinterpreting the solidification temperatures of Ronchi and Hiernaut on the basis of their published thermogram in the same way as thermograms in this work have been interpreted, one reaches a temperature of 3639 K ± 42 K (only the data spread with a 2-k coverage factor is considered), which is even closer to our result of 3624 K. Other effects as the reported pre-melting transition were not seen in the current study. Generally, small enthalpy changes are not expected to be seen with the experimental approach in this work, due to the different sample geometry and heat loss balance with respect to Ronchi and Hiernaut's work.

The interpretation of the thermograms has been already discussed in a previous work with the help of Phase-Field simulations [18], which show that the complex shape of the thermal arrest comes from rapid solidification of the surface rather than a solidus/liquidus transition in thermodynamic equilibrium. Compared to the diffusion rates of actinide oxides [43] the solidification process in these experiments is very fast, so that an exact identification of the liquidus (first appearance of solid in the molten zone) and solidus (solidification of the last molten material) temperatures becomes very difficult [45]. With the help of the reflected light signal, the melting transition could be identified in some measurements and was found to be close to the solidification temperature as one can see in Fig. 3 and Fig. 8. The differences are still within the uncertainty bands. The most likely explanation for this melting/solidification difference is parasite reflections of the heating laser into the pyrometer.

The UO_2–ThO_2 system is an isomorphous binary phase diagram. In this kind of system only one solid phase exists at the equilibrium and the two endmembers exhibit a complete solid solubility. If one assumes ideal solid and liquid solutions for every composition, solidus and liquidus can be calculated solely based on the thermodynamic data of the two end members recently reviewed by Konings et al. [46] and considering only ideal configurational entropy contributions. The resulting solidus and liquidus plots are shown in Fig. 8 together with the current and literature experimental data.

The minimum melting temperature found in this work for 5 mol% ThO_2 contradicts a fully ideal solution in the domain of melting (as already graphically assumed by Belle and Berman [5]). The work of Lambertson et al. [11] showed a total miscibility of the components in all proportions. Latta et al. [12] focused their attention on the region below 20 mol% ThO_2, for which a minimum at 5 mol% ThO_2 was also observed. The melting temperatures in that study are similar to this work in the uranium rich part, but differ

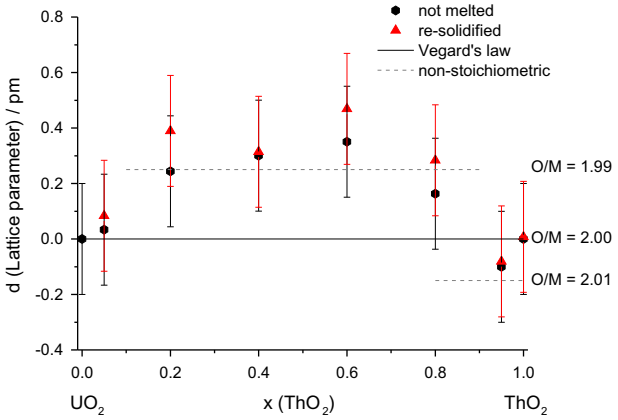

Fig. 7. Difference between lattice parameters of the samples (±0.002 Å) and Vegard's law interpolation between the endmembers in dependence of the ThO_2 content. The black line represents Vegard's law between the stoichiometric UO_2 and ThO_2. The dotted lines suggest non-stoichiometric changes from hyperstoichiometric studies on (U, Th)O_2 [42] and hypostoichiometric studies on (U, Pu)O_2 [43].

in the intermediate compositions. In the thorium rich part of the phase diagram data are more rare, so that a direct comparison of each composition is not possible. This deviation from ideal behaviour close to UO_2, the chemically less stable oxide, emphasises a stabilizing effect of ThO_2 in mixed actinide oxides [42]. The reproducibility by laser containerless heating of older data with a high content of thoria confirms that the oxygen potential is indeed a crucial parameter determining the reactivity of these oxides with the containment.

With the used characterisation methods, small variations between the re-solidified and the not melted material can be linked to segregation on the most external part of the freezing surface. According to the phase diagram the composition formed at the liquidus temperature upon solidification of the sample surface corresponds to the solidus point of another composition enriched in ThO_2. This latter surface composition is likely to be quenched to room temperature almost unchanged, due to slower mass diffusion in the solid. Therefore it is suggested to move the observed solidification points of the intermediate compositions (20, 40 and 60 mol% ThO_2) towards the ThO_2 side of the phase diagram (see Fig. 8), although the shift could not be exactly quantified. Thus, ideal solution behaviour can be approximated for most of the compositions.

Calphad optimisation of phase diagrams of actinide oxides suggest a non-congruent (slightly hypostoichiometric) melting for dioxides [21,19], and oxygen potential studies of hyperstoichiometric (U, Th)O_2 suggested a non-ideal hyperstoichiometric system [47].

Almost ideal solid solution behaviour has been observed in most compositions in this study, especially for thorium rich compositions. The slight deviation from the ideal solution leading to a minimum melting point in the UO_2-rich part can be fairly reproduced by using a polynomial formalism of the type proposed by Pelton and Thompson [48], with one adjustable parameter for describing the excess Gibbs energy ΔG^{exc} in the solid:

$$\Delta G^{exc} = x(UO_2)^4 \cdot x(ThO) \cdot A \quad (1)$$

A is a parameter, assumed to be temperature-independent, representing the interaction between the components in the solid solution. The exponents with which the molar fractions of urania and thoria ($x(UO_2)$ and $x(ThO_2)$ respectively) appear in Eq. 1 account for asymmetry in the model, consistently with the most relevant deviations from ideality observed in uranium-richer compositions. In this first-approach excess parameter optimization, the liquid phase is still treated as a fully ideal solution. Best fit of the experimental solidification data (considered as solidus points at compositions corrected for eventual segregation effects) was obtained for A = 25 kJ mol^{-1}. The resulting solidus and liquidus lines are also reported in Fig. 8 (solid curves). They do match a minimum melting point for low thoria contents. They also seem to be more consistent with the mentioned shifts induced in intermediate compositions by segregation effects during the melting/freezing process and with earlier solidus data [11,12]. A plot of the relative solid mixing (excess) enthalpy $\Delta_{mix}H$ vs. composition is reported in the inset of Fig. 8. These results are obtained in a first-approximation approach, and should therefore be considered as purely indicative of general trends. Nonetheless, they do give a rough quantification of deviations from ideal solution behaviour concentrated in urania-rich compositions. Such deviations can be certainly related to the formation of lattice defects for high UO_2 contents. In these compositions, the formation of both oxygen interstitials and vacancies is very likely due to the possibility for uranium to assume, in the oxide, the valence states +3, +4, +5 and +6, whereas thorium is stable only in the form Th^{4+} [43]. This is also in line with the current Raman analysis, which showed that further oxidised structures of UO_2 are more easily formed on the surface of samples with nominally 5 and 20 mol% ThO_2, i.e. for the lowest ThO_2 contents investigated here.

Interestingly, a small addition of ThO_2 to UO_2 seems to still permit the formation of these structures rather than hindering it. The uranium rich part of the system can therefore be fully assessed only as a ternary U–Th–O. This behaviour can also be described, in a first approximation, as a binary non-stoichiometric phase diagram as shown in [18]. In the light of such behaviour, it is easier to understand the anomalous melting point deviation from the ideal solidus and liquidus lines in mixed uranium–thorium dioxides with low thorium content.

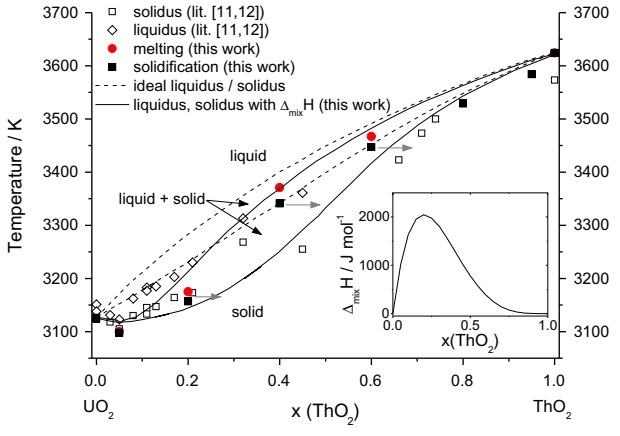

Fig. 8. High temperature phase diagram of the pseudo-binary UO_2–ThO_2 system. Results of this work are shown together with the ideal solution binary solidus and liquidus (solid lines) and data from earlier measurements [11,12]. With grey arrows a suggested shift of the obtained melting/solidification temperatures is shown qualitatively. The solid solidus and liquidus lines take into account deviations from the ideal solution behaviour. They have been calculated by considering a mixing enthalpy in the solid solution, whose values reported in the inset have been optimised in order to best fit the current experimental data with a polynomial formalism.

5. Conclusions

Following novel results in disagreement to earlier data found for pure and mixed actinide oxides with containerless laser heating, this study re-analysed ThO_2 and the mixed system (U, Th)O_2. Several conclusions can be drawn from these experiments:

- With respect to the high temperature interaction between sample and containment, the reproducibility of earlier results seems to be better in compounds like ThO_2, with a low oxygen potential. Earlier results were reproduced within the uncertainty bands, confirming a minimum melting point in the UO_2–ThO_2 system around 5 mol% ThO_2 and 3098 K.
- The (U, Th)O_2 system should be described, in the uranium rich part, rather as a ternary U–Th–O system than a purely pseudo-binary UO_2–ThO_2. The performed material analyses (SEM, Raman spectroscopy, XRD) support this interpretation, by showing the formation, on the very surface of the re-solidified sample, of species with a higher oxidation state only for thorium dioxide concentrations lower than approximately 20 mol% ThO_2. More effects at high temperature, as e.g. defect formation and O/M variations, may play a further role, but could not be identified with the current analysis methods at room temperature.
- Ideal solution behaviour can be reasonably hypothesised around melting for intermediate and ThO_2-rich compositions. Based on material characterisation results, segregation effects cannot be excluded on the observed melting/solidification temperatures of intermediate compositions (20, 40 and 60

mol% ThO_2). These compositions show by bulk and thermal analysis only minor differences between re-solidified and not melted material. Surface analysis (Raman spectroscopy) reveals possible composition shifts, difficult to quantify. These shifts are probably limited to the very surface of the re-solidified sample and are in line with a quenching solidification process in the phase diagram.

The current results help to understand the high temperature behaviour of a refractory material in terms of basic research and also in terms of safety and security of a possible nuclear fuel in accidental or operating conditions.

Acknowledgements

The Authors are indebted to P. Raison, G. Pagliosa, D. Bouexière, B. Cremer, A. Janssen (all JRC-ITU) for their precious help in the sample characterisation. This work is funded by the European Commission and partly supported by E.ON Kernkraft GmbH via contract no. 32920.

References

[1] P.R. Hania, F.C. Klaassen, 3.04 - Thorium oxide fuel, in: R.J.M. Konings (Ed.), Compr. Nucl. Mater, Elsevier, Oxford, 2012, pp. 87–108, http://dx.doi.org/10.1016/B978-0-08-056033-5.00052-5.
[2] S.F. Ashley, G.T. Parks, W.J. Nuttall, C. Boxall, R.W. Grimes, Nuclear energy: thorium fuel has risks, Nature 492 (7427) (2012) 31–33, http://dx.doi.org/10.1038/492031a.
[3] W.E. Lee, M. Gilbert, S.T. Murphy, R.W. Grimes, Opportunities for advanced ceramics and composites in the nuclear sector, J. Am. Ceram. Soc. 96 (7) (2013) 2005–2030, http://dx.doi.org/10.1111/jace.12406.
[4] C. Lombardi, L. Luzzi, E. Padovani, F. Vettraino, Thoria and inert matrix fuels for a sustainable nuclear power, Prog. Nucl. Energy 50 (8) (2008) 944–953, http://dx.doi.org/10.1016/j.pnucene.2008.03.006.
[5] J. Belle, R. Berman, Thorium dioxide: properties and nuclear applications, Tech. rep., USDOE Office of Nuclear Energy, Science and Technology (NE) (Jan. 1984). doi:10.2172/5986642.
[6] J. Herring, P.E. MacDonald, K.D. Weaver, C. Kullberg, Low cost, proliferation resistant, uranium–thorium dioxide fuels for light water reactors, Nucl. Eng. Des. 203 (1) (2001) 65–85, http://dx.doi.org/10.1016/S0029-5493(00)00297-1.
[7] M. Basu (Ali), R. Mishra, S. Bharadwaj, D. Das, Thermodynamic and transport properties of thoria–urania fuel of advanced heavy water reactor, J. Nucl. Mater. 403 (1-3) (2010) 204–215, http://dx.doi.org/10.1016/j.jnucmat.2010.01.009.
[8] Y. Lu, Y. Yang, P. Zhang, Thermodynamic properties and structural stability of thorium dioxide, J. Phys. Condens. Matter 24 (22) (2012) 225801, http://dx.doi.org/10.1088/0953-8984/24/22/225801.
[9] O. İpek, Analysis of temperature distribution, burn-up and breeding parameters in nuclear fuel rod in fusion-fission reactor system fueled with mixed ThO_2–UO_2 fuel, Int. J. Energy Res. 35 (2) (2011) 112–122, http://dx.doi.org/10.1002/er.1771.
[10] C. Lombardi, L. Luzzi, E. Padovani, F. Vettraino, Inert matrix and thoria fuels for plutonium elimination, Prog. Nucl. Energy 38 (3-4) (2001) 395–398, http://dx.doi.org/10.1016/S0149-1970(00)00143-8.
[11] W.A. Lambertson, M.H. Mueller, F.H. Gunzel, Uranium oxide phase equilibrium systems: IV, UO_2–ThO_2, J. Am. Ceram. Soc. 36 (12) (1953) 397–399, http://dx.doi.org/10.1111/j.1151-2916.1953.tb12827.x.
[12] R. Latta, E. Duderstadt, R. Fryxell, Solidus and liquidus temperatures in the UO_2–ThO_2 system, J. Nucl. Mater. 35 (3) (1970) 347–349, http://dx.doi.org/10.1016/0022-3115(70)90219-9.
[13] D. Manara, C. Ronchi, M. Sheindlin, M. Lewis, M. Brykin, Melting of stoichiometric and hyperstoichiometric uranium dioxide, J. Nucl. Mater. 342 (1-3) (2005) 148–163, http://dx.doi.org/10.1016/j.jnucmat.2005.04.002.
[14] C. Ronchi, J.-P. Hiernaut, Experimental measurement of pre-melting and melting of thorium dioxide, J. Alloys Comp. 240 (1-2) (1996) 179–185, http://dx.doi.org/10.1016/0925-8388(96)02329-8.
[15] F. De Bruycker, K. Boboridis, D. Manara, P. Pöml, M. Rini, R.J. Konings, Reassessing the melting temperature of PuO_2, Mater. Today 13 (11) (2010) 52–55, http://dx.doi.org/10.1016/S1369-7021(10)70204-2.
[16] R. Böhler, M.J. Welland, F.D. Bruycker, K. Boboridis, A. Janssen, R. Eloirdi, R.J.M. Konings, D. Manara, Revisiting the melting temperature of NpO_2 and the challenges associated with high temperature actinide compound measurements, J. Appl. Phys. 111 (11) (2012) 113501, http://dx.doi.org/10.1063/1.4721655.
[17] F. De Bruycker, K. Boboridis, R. Konings, M. Rini, R. Eloirdi, C. Guéneau, N. Dupin, D. Manara, On the melting behaviour of uranium/plutonium mixed dioxides with high-Pu content: a laser heating study, J. Nucl. Mater. 419 (1-3) (2011) 186–193, http://dx.doi.org/10.1016/j.jnucmat.2011.08.028.
[18] R. Böhler, M. Welland, D. Prieur, P. Cakir, T. Vitova, T. Pruessmann, I. Pidchenko, C. Hennig, C. Guéneau, R. Konings, D. Manara, Recent advances in the study of the UO_2–PuO_2 phase diagram at high temperatures, J. Nucl. Mater. 448 (1-3) (2014) 330–339, http://dx.doi.org/10.1016/j.jnucmat.2014.02.029.
[19] C. Guéneau, N. Dupin, B. Sundman, C. Martial, J.-C. Dumas, S. Gossé, S. Chatain, F.D. Bruycker, D. Manara, R.J. Konings, Thermodynamic modelling of advanced oxide and carbide nuclear fuels: description of the U–Pu–O–C systems, J. Nucl. Mater. 419 (1-3) (2011) 145–167, http://dx.doi.org/10.1016/j.jnucmat.2011.07.033.
[20] D. Manara, R. Böhler, K. Boboridis, L. Capriotti, A. Quaini, L. Luzzi, F. De Bruycker, C. Guéneau, N. Dupin, R. Konings, The melting behaviour of oxide nuclear fuels: effects of the oxygen potential studied by laser heating, Procedia Chem. 7 (2012) 505–512, http://dx.doi.org/10.1016/j.proche.2012.10.077.
[21] H. Kinoshita, D. Setoyama, Y. Saito, M. Hirota, K. Kurosaki, M. Uno, S. Yamanaka, Thermodynamic modelling and phase stability assessment of MO_{2-x} oxides with a fluorite structure, J. Chem. Thermodyn. 35 (5) (2003) 719–731, http://dx.doi.org/10.1016/S0021-9614(03)00002-8.
[22] C. Jégou, R. Caraballo, S. Peuget, D. Roudil, L. Desgranges, M. Magnin, Raman spectroscopy characterization of actinide oxides $(U_{1-y}Pu_y)O_2$: resistance to oxidation by the laser beam and examination of defects, J. Nucl. Mater. 405 (3) (2010) 235–243, http://dx.doi.org/10.1016/j.jnucmat.2010.08.005.
[23] M.J. Sarsfield, R.J. Taylor, C. Puxley, H.M. Steele, Raman spectroscopy of plutonium dioxide and related materials, J. Nucl. Mater. 427 (1-3) (2012) 333–342, http://dx.doi.org/10.1016/j.jnucmat.2012.04.034.
[24] D. Manara, M. Sheindlin, W. Heinz, C. Ronchi, New techniques for high-temperature melting measurements in volatile refractory materials via laser surface heating, Rev. Sci. Instrum. 79 (11) (2008) 113901, http://dx.doi.org/10.1063/1.3005994.
[25] H. Preston-Thomas, The international temperature scale of 1990 (ITS-90), Metrologia 27 (1) (1990) 3–10, http://dx.doi.org/10.1088/0026-1394/27/1/002.
[26] R.E. Bedford, G. Bonnier, H. Maas, F. Pavese, Recommended values of temperature on the international temperature scale of 1990 for a selected set of secondary reference points, Metrologia 33 (2) (1996) 133–154, http://dx.doi.org/10.1088/0026-1394/33/2/3.
[27] F. De Bruycker, K. Boboridis, P. Pöml, R. Eloirdi, R. Konings, D. Manara, The melting behaviour of plutonium dioxide: a laser-heating study, J. Nucl. Mater. 416 (1-2) (2011) 166–172, http://dx.doi.org/10.1016/j.jnucmat.2010.11.030.
[28] M. Bober, J. Singer, K. Wagner, Spectral Reflectivity and Emissivity Measurements of Solid and Liquid UO_2 at 458, 514.5 and 647 nm as a Function of Polarization and Angle of Incidence, Tech. Rep. September, Kernforschungszentrum Karlsruhe - Institut für Neutronenphysik und Reaktortechnik (1980).
[29] H. Karow, M. Bober, Experimental investigations into the spectral relectivities and emissivities of liquid UO_2 , UC, ThO_2 , and Nd_2O_3, Thermodyn. Nucl. Mater. 1979, Vol. 1, IAEA, 1980, pp. 155–169.
[30] D. Manara, R. Böhler, L. Capriotti, A. Quaini, Z. Bao, K. Boboridis, L. Luzzi, A. Janssen, P. Pöml, R. Eloirdi, R. Konings, On the melting behaviour of calcium monoxide under different atmospheres: a laser heating study, J. Eur. Ceram. Soc. 34 (6) (2014) 1623–1636, http://dx.doi.org/10.1016/j.jeurceramsoc.2013.12.018.
[31] G. Begun, R. Haire, W. Wilmarth, J. Peterson, Raman spectra of some actinide dioxides and of EuF_2, J. Less Common Met. 162 (1) (1990) 129–133, http://dx.doi.org/10.1016/0022-5088(90)90465-V.
[32] T. Livneh, E. Sterer, Effect of pressure on the resonant multiphonon Raman scattering in UO_2, Phys. Rev. B 73 (8) (2006) 085118, http://dx.doi.org/10.1103/PhysRevB.73.085118.
[33] L. Desgranges, G. Guimbretière, P. Simon, C. Jegou, R. Caraballo, A possible new mechanism for defect formation in irradiated UO_2, Nucl. Instrum. Methods Phys. Res. Sect. B Beam Interact. Mater. Atoms 315 (2013) 169–172, http://dx.doi.org/10.1016/j.nimb.2013.05.081.
[34] L. Desgranges, G. Baldinozzi, P. Simon, G. Guimbretière, A. Canizares, Raman spectrum of U_4O_9: a new interpretation of damage lines in UO_2, J. Raman Spectrosc. 43 (3) (2012) 455–458, http://dx.doi.org/10.1002/jrs.3054.
[35] F. Pointurier, O. Marie, Identification of the chemical forms of uranium compounds in micrometer-size particles by means of micro-Raman spectrometry and scanning electron microscope, Spectrochim. Acta Part B At. Spectrosc. 65 (9-10) (2010) 797–804, http://dx.doi.org/10.1016/j.sab.2010.06.008.
[36] R. Rao, R.K. Bhagat, N.P. Salke, A. Kumar, Raman spectroscopic investigation of thorium dioxide-uranium dioxide (ThO_2–UO_2) fuel materials, Appl. Spectrosc. 68 (1) (2014) 44–48, http://dx.doi.org/10.1366/13-07172.
[37] V.G. Keramidas, Raman spectra of oxides with the fluorite structure, J. Chem. Phys. 59 (3) (1973) 1561, http://dx.doi.org/10.1063/1.1680227.
[38] M. Ishigame, M. Kojima, Second-order raman spectra of thorium dioxide, J. Phys. Soc. Japan 41 (1) (1976) 202–210, http://dx.doi.org/10.1143/JPSJ.41.202.
[39] M.T. Hutchings, High-temperature studies of UO_2 and ThO_2 using neutron scattering techniques, J. Chem. Soc., Faraday Trans. 2 83 (7) (1987) 1083–1103, http://dx.doi.org/10.1039/F29878301083.
[40] R.J. Ackermann, R.J. Thorn, G.H. Winslow, Visible and ultraviolet absorption properties of uranium dioxide films, J. Opt. Soc. Am. 49 (11) (1959) 1107, http://dx.doi.org/10.1364/JOSA.49.001107.
[41] O. Weinreich, W. Danforth, Optical properties of crystalline thoria, Phys. Rev. 88 (4) (1952) 953–954, http://dx.doi.org/10.1103/PhysRev.88.953.2.
[42] I. Cohen, R. Berman, A metallographic and X-ray study of the limits of oxygen solubility in the UO_2–ThO_2 system, J. Nucl. Mater. 18 (2) (1966) 77–107, http://dx.doi.org/10.1016/0022-3115(66)90073-0.

[43] C. Guéneau, A. Chartier, L.V. Brutzel, 2.02 - Thermodynamic and thermophysical properties of the actinide oxides, in: R.J. Konings (Ed.), Compr. Nucl. Mater, Elsevier, Oxford, 2012, pp. 21–59, http://dx.doi.org/10.1016/B978-0-08-056033-5.00009-4.

[44] S. Hubert, J. Purans, G. Heisbourg, P. Moisy, N. Dacheux, Local structure of actinide dioxide solid solutions $Th_{1-x}U_xO_2$ and $Th_{1-x}Pu_xO_2$, Inorg. Chem. 45 (10) (2006) 3887–3894, http://dx.doi.org/10.1021/ic050888y.

[45] M.J. Aziz, T. Kaplan, Continuous growth model for interface motion during alloy solidification, Acta Metall. 36 (8) (1988) 2335–2347, http://dx.doi.org/10.1016/0001-6160(88)90333-1.

[46] R.J.M. Konings, O. Beneš, A. Kovács, D. Manara, D. Sedmidubský, L. Gorokhov, V.S. Iorish, V. Yungman, E. Shenyavskaya, E. Osina, The thermodynamic properties of the f-elements and their compounds. Part 2. the lanthanide and actinide oxides, J. Phys. Chem. Ref. Data 43 (1) (2014) 013101, http://dx.doi.org/10.1063/1.4825256.

[47] M. Ugajin, Oxygen potentials of (Th, U)O_{2+x} solid solutions, J. Nucl. Mater. 110 (2-3) (1982) 140–146, http://dx.doi.org/10.1016/0022-3115(82)90138-6.

[48] A. Pelton, W. Thompson, Phase diagrams, Prog. Solid State Chem. 10 (1975) 119–155, http://dx.doi.org/10.1016/0079-6786(75)90004-7.